Conformal Surface Coatings to Enable High Volume Expansion Li-Ion Anode Materials

Leah A. Riley,[a, b] Andrew S. Cavanagh,[c] Steven M. George,[d] Yoon Seok Jung,[a] Yanfa Yan,[a] Se-Hee Lee,[b] and Anne C. Dillon*[a]

An alumina surface coating is demonstrated to improve electrochemical performance of MoO_3 nanoparticles as high capacity/high-volume expansion anodes for Li-ion batteries. Thin, conformal surface coatings were grown using atomic layer deposition (ALD) that relies on self-limiting surface reactions. ALD coatings were tested on both individual nanoparticles and prefabricated electrodes containing conductive additive and binder. The coated and non-coated materials were characterized using transmission electron microscopy, energy-dispersive X-ray spectroscopy, electrochemical impedance spectroscopy, and galvanostatic charge/discharge cycling. Importantly, increased stability and capacity retention was only observed when the fully fabricated electrode was coated. The alumina layer both improves the adhesion of the entire electrode, during volume expansion/contraction and protects the nanoparticle surfaces. Coating the entire electrode also allows for an important carbothermal reduction process that occurs during electrode pre-heat treatment. ALD is thus demonstrated as a novel and necessary method that may be employed to coat the tortuous network of a battery electrode.

1. Introduction

For several decades, lithium-ion battery technologies have evolved with significant advancements in both stability and efficiency achieved. However, the commercial graphitic anodes for lithium-ion batteries are limited to a specific capacity of ~ 350 mAh g^{-1}. Furthermore, graphitic anodes, which typically operate at a potential of ~ 0.1 V vs Li/Li$^+$, also do not meet the suggested HEV battery operating potential of ~ 0.5 V vs Li/Li$^+$ that will mitigate Li-plating and eliminate safety concerns.[1] Thus, current technology is not suitable for high-performance applications including hybrid electric vehicles and plug-in hybrid electric vehicles (HEVs and PHEVs) that require higher energy and power densities as well as longer lifetimes. Hence, modern battery research is committed to develop a high-capacity alternative to graphite. Recently silicon and metal oxides have been significantly studied as they offer the potential of highly increased capacity. In contrast to the well-studied lithium intercalation mechanism of graphite, lithiation of crystalline silicon leads to the formation of a metastable amorphous alloy, sustaining up to 4.4 Li$^+$ per Si.[2] Transition metal oxides undergo a conversion reaction at lower voltages, yielding pure metal and Li$_2$O as shown in Equation (1).[3]

$$MO_x + 2x\,Li^+ + 2x\,e^- \rightarrow x\,Li_2O + M \qquad (1)$$
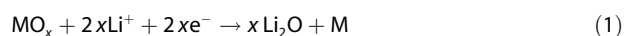
However, for materials, such as silicon and transition metal oxides, which can accommodate more than 4 Li$^+$/formula unit, extreme volume changes ($>100\%$) occur resulting in fracturing and loss of electrical conductivity and mechanical integrity with a subsequent rapid fade in capacity.

In order to mitigate capacity degradation, researchers have employed various nanostructures that may better accommodate volume strain. Many methods employ alternative binder-free and 3-D cell constructions, such as thin film,[4–6] nano-arrays,[7–9] and embedded composites and membranes.[10,11] Although higher reversible capacities using alternative cell architectures have been achieved, most of these formats are not yet plausible for large scale, commercial, roll-to-roll processing.

High-volume expansion materials have also been demonstrated using conventional (more commercially applicable) slurries of active material, conductive additive, and binder spread onto a current collector. For example, Lui et al. used hydrothermally synthesized α-Fe$_2$O$_3$ nanorods in a conventional slurry to dramatically increase capacity, from 112 to 763 mAh g^{-1} after 30 cycles, compared to that of commercially available material.[12] In addition, Beattie et al. maintained close to silicon's theoretical capacity (4200 mAh g^{-1}) for 20 cycles

[a] L. A. Riley, Dr. Y. S. Jung, Dr. Y. Yan, Dr. A. C. Dillon
Materials Science Center
National Renewable Energy Laboratory
1617 Cole Boulevard, Golden, CO 80401 (USA)
Fax: (+1) 303 384 7600
E-mail: anne.dillon@nrel.gov

[b] L. A. Riley, Dr. S.-H. Lee
Department of Mechanical Engineering
University of Colorado at Boulder
427 UCB, Boulder, CO 80309 (USA)

[c] A. S. Cavanagh
Department of Physics
University of Colorado at Boulder
Boulder, CO 80309 (USA)

[d] Dr. S. M. George
Department of Chemistry and
Biochemistry of Chemical and Biochemical Engineering
University of Colorado at Boulder
Boulder, CO 80309-0215 (USA)

Report Documentation Page		*Form Approved* *OMB No. 0704-0188*
Public reporting burden for the collection of information is estimated to average 1 hour per response, including the time for reviewing instructions, searching existing data sources, gathering and maintaining the data needed, and completing and reviewing the collection of information. Send comments regarding this burden estimate or any other aspect of this collection of information, including suggestions for reducing this burden, to Washington Headquarters Services, Directorate for Information Operations and Reports, 1215 Jefferson Davis Highway, Suite 1204, Arlington VA 22202-4302. Respondents should be aware that notwithstanding any other provision of law, no person shall be subject to a penalty for failing to comply with a collection of information if it does not display a currently valid OMB control number.		

1. REPORT DATE **2010**	2. REPORT TYPE	3. DATES COVERED **00-00-2010 to 00-00-2010**
4. TITLE AND SUBTITLE **Conformal Surface Coatings to Enable High Volume Expansion Li-Ion Anode Materials**		5a. CONTRACT NUMBER
		5b. GRANT NUMBER
		5c. PROGRAM ELEMENT NUMBER
6. AUTHOR(S)		5d. PROJECT NUMBER
		5e. TASK NUMBER
		5f. WORK UNIT NUMBER
7. PERFORMING ORGANIZATION NAME(S) AND ADDRESS(ES) **University of Colorado,Department of Chemistry and Biochemistry,Boulder,CO,80309**		8. PERFORMING ORGANIZATION REPORT NUMBER
9. SPONSORING/MONITORING AGENCY NAME(S) AND ADDRESS(ES)		10. SPONSOR/MONITOR'S ACRONYM(S)
		11. SPONSOR/MONITOR'S REPORT NUMBER(S)

12. DISTRIBUTION/AVAILABILITY STATEMENT **Approved for public release; distribution unlimited**
13. SUPPLEMENTARY NOTES
14. ABSTRACT
15. SUBJECT TERMS

16. SECURITY CLASSIFICATION OF:			17. LIMITATION OF ABSTRACT	18. NUMBER OF PAGES	19a. NAME OF RESPONSIBLE PERSON
a. REPORT **unclassified**	b. ABSTRACT **unclassified**	c. THIS PAGE **unclassified**	**Same as Report (SAR)**	**7**	

Standard Form 298 (Rev. 8-98)
Prescribed by ANSI Std Z39-18

using commercial nanopowder in a conventional format. However, in each example, enhanced performance could only be obtained by adding large quantities of conductive additive and binder to maintain electrical conductivity, and cutting down the active material to ≤ 40 wt.% to allow for volume expansion. Li et al. demonstrated that binder choice and electrode pre-heat treatment could stabilize μ-sized particles of α-Fe_2O_3 with an active material loading of 80% but required cycling at a lower rate of C/5 (five hours each for charge and discharge).[13]

In order to accommodate for the high volume expansion of silicon, Kang et al. coated Si particles with Co–Co_3O_4 by sol-gel.[14] The coating improved the 12th cycle efficiency from 55% to 88% for micron-sized particles. While appropriate for larger particles, the coating was comprised of particulates ranging from 0.1 to 1 micron in diameter. Thus the coating itself is larger than most nanomaterials. For thin conformal coatings (Å-level control) Jung et al. demonstrated atomic layer deposition (ALD) as a promising alternative for surface passivation that maximizes active material loading.[15] ALD grown coatings have also been shown to grow deep within porous structures of prefabricated electrodes.[16]

The layered structure of α-MoO_3 was first proposed as a material of interest for Li-ion batteries as a cathode in the 1970s,[17] but was not demonstrated as an anode material due to the volume expansion occurring for high Li-loading at lower potential. Using nanoparticle α-MoO_3 for an anode, we previously demonstrated an anomalous reversible capacity as a thin film electrode and then achieved improved reversible capacity (~1000 mAh g^{-1}) in a traditional electrode architecture.[18, 19] Our electrode composition contained only 10 wt.% conductive additive, 20 wt.% binder and 70 wt.% active material. We also established a necessary electrode heat treatment at 250 °C, unique to MoO_3, that enabled both carbothermal reduction, and electrode adhesion via binder melting without early onset of binder breakdown. Both the cycle life and capacity were then improved despite the volume change, with minimal additives. However, stable cycling was only observed at a lower rate of C/10 (10 h each for charge and discharge).

Our current work focuses on improving the durable high-rate capability of high volume expansion nanoparticle MoO_3 conventional anodes by applying a thin coating of alumina on the electrode surface using atomic layer deposition (ALD). Unlike the sol-gel methods that have been previously employed, ALD is a "dry" process that can be easily applied to full electrodes and allows for very thin conformal films to be deposited. By coating the full electrode the ALD coating appears to "knit" the active material to the conductive additive thereby preserving mechanical integrity during volume expansion/contraction. The ALD coating also protects the high surface area of the nanoparticles from decomposition and reaction with the liquid electrolyte. Finally, full electrode coating allows for pre-heat treatments that enable important interactions between the active material and additives to be achieved. Ultimately improved durability at high rates is demonstrated. When ALD is performed directly on the particles rather than on the composite electrodes, superior performance is not achieved. Impor-

tantly, we note that it is not possible to employ sol gel techniques on composite electrodes.

2. Results and Discussion

As discussed previously in detail,[18–20] the crystalline MoO_3 is grown using a unique hot-wire chemical vapor deposition (HWCVD) technique. In this study, self-limiting ALD is performed using trimethylaluminum (TMA) and H_2O precursors. Unlike wet-chemical techniques, ALD precursors can easily traverse tortuous paths within porous structures, providing a uniform coating on all exposed surfaces. Likewise, by using a rotary reactor, uniform growth can also be achieved on individual particles. One ALD cycle consists of TMA exposure, a purge, and H_2O exposure. Each complete deposition cycle of ALD grows ~1–2 Å of Al_2O_3 on porous surfaces and powders. Additional layers are grown by repeating the ALD cycle. Alumina grown by ALD has been shown to have 75% the density of bulk amorphous alumina.[21] A transmission electron microscope (TEM) image of a bare MoO_3 nanoparticle (prior to the application of an ALD coating) is shown in Figure 1a. The elemental composition of the circular area labeled P1 was examined using energy dispersive X-ray spectroscopy (EDS) to verify that no aluminum was present before ALD (Figure 1b). Figure 1c is a TEM image of a MoO_3 nanoparticle coated with 4-cycles of TMA/H_2O, resulting in a thin coating of alumina. The crystalline structure for the MoO_3 nanoparticles is apparent in both Figures 1a and c. However for the coated particle (Figure 1c), a thin, bright white surface film, less than 1 nm in thickness, is visible that is absent from the bare powder. EDS of the ALD surface region in the identical location as on the
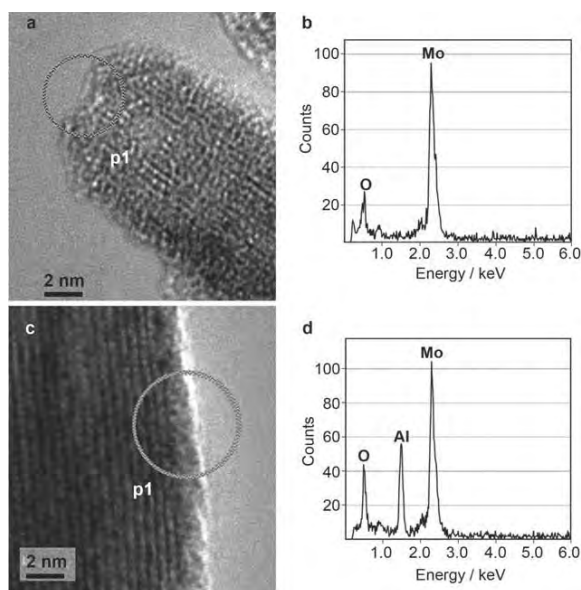

Figure 1. a) TEM of bare MoO_3 nanoparticle. b) EDS of the circular area marked p1 shows no aluminum present on the surface of the bare sample. c) TEM of a MoO_3 nanoparticle coated by ALD with 4 monolayers of Al_2O_3 on the surface. d) EDS of area labeled as p1 confirms the presence of alumina at a mono-layer level.

bare sample confirms that the bright film is a very thin layer of Al_2O_3 upon the surface of the nanoparticle (Figure 1d). Note that the ALD coating also appears to improve the surface roughness of the particles.

Electrochemical capacity and stability comparisons for bare MoO_3 electrodes, ALD coated MoO_3 nanoparticles (CP) electrodes, and ALD coated nano-MoO_3 electrodes (CE) are depicted in Figure 2a. All electrodes were of a 70:10:20 composition active material (AM):acetylene black (AB):binder (PVDF) and subjected to 250 °C heat treatment. For electrodes comprised of CP, an alumina surface layer was grown on MoO_3 particles prior to coin cell fabrication, leaving the carbon additive and binder uncoated. Conversely, ALD was also applied after electrode fabrication, coating all exposed electrode surfaces and pores, to make the CE. The dotted horizontal line at 1117 mAh g^{-1} represents the theoretical maximum capacity of MoO_3 when completely lithiated [6 Li$^+$ per MoO_3 formula unit as given by Eq. (1)]. After the first two cycles at C/10, each sample is cycled at a rate of C/2 (only 2 h for each charge and discharge) from 3.0 to 0.001 V at room temperature. As shown in Figure 2a, the bare MoO_3 nanoparticles exhibit a progressive capacity fade after only 15 cycles. Consistent with the onset of stability loss, the coulombic efficiency of the electrode also degrades (Figure 2b). The gradual capacity loss and poor efficiency is attributed primarily to mechanical degradation due to volume expansion with surface decomposition/reaction with the liquid electrolyte also playing a role. Interestingly, individual nanoparticles coated with 4 cycles of Al_2O_3 ALD show inferior performance to the bare nano-MoO_3 (Figure 2a) as the cou-

lombic efficiency drops from 74 % to 63 % in the first cycle (Figure 2b). The CP then exhibits a rapid drop in capacity upon further cycling, finally stabilizing around the 10th cycle, with a low reversible capacity of ~380 mAh g^{-1}.

Unlike the individual particle coated sample, dramatically improved cycling performance is observed (Figure 2a) when the entire electrode is coated with 4 cycles of Al_2O_3 ALD. The CE shows no capacity fade for over 50 cycles at C/2 rate and maintains a stable reversible capacity of 900 mAh g^{-1} corresponding to an uptake of 4.8 Li$^+$/MoO_3. By the 40th cycle the coulombic efficiency of the electrode coated sample is 97.5 % compared to the bare sample with a coulombic efficiency of 94 %. The improved durability of the ALD coated electrodes is even more dramatically depicted by exploring the rate capability as depicted in Figure 2c. At a rate of 2C (30 min for both charge and discharge) the surface coated electrode delivers a capacity of nearly 800 mAh g^{-1} while the bare exhibits only 400 mAh g^{-1}. Also the coated electrode delivers ~600 mAh g^{-1} in only 12 min when cycled at 5 C. Thus, and perhaps surprisingly, the electrode coating provides beneficial protection against capacity degradation while the individual particle coating appears detrimental to overall performance. The voltage profiles depicted in Figure 2d compare the 1st cycle (C/10) to the 40th cycle (C/2) for the very stable ALD coated electrode sample. Despite the increase in current density, the extraction profiles are nearly identical after 40 cycles (although an irreversible capacity loss is observed in the first insertion cycle). The 4th cycle is also shown to demonstrate consistency in the voltage profiles when cycling at the same rate.

In a recent study, Miller et al. found that a 5 nm ALD alumina surface coating deforms elastically up to ~2 % strain and that the critical strain for steady state channel crack propagation occurs at ~5.1 %.[22] Using these findings as a guide, the theoretical strain of alumina surface coatings when applied to various active materials is calculated in Table 1. Alumina coatings on materials which experience small changes in volume, such as $LiCoO_2$, remain in the elastic region of deformation and are obviously relevant to the work of Jung et al.[15] In this report the $LiCoO_2$ was cycled up to 4.5 V vs Li/Li$^+$ where cobalt dissolution and oxidative decomposition of the electrolyte are known to occur. Thus the Al_2O_3 definitely served as a protective coating.[16] However, for high volume expansion materials, such as MoO_3, at least a 100 % volume change during lithiation occurs corresponding to a strain of 26 %, that must induce cracking and fracturing along the protective surface layer. It is thus somewhat surprising that the ALD coatings improve the cycling performance of the high volume expansion materials, when mechanical integrity is usually lost upon cycling. A schematic of the expansion effects for bare, CP, and CE is depicted in Figures 3a–c. The white circles represent MoO_3 nanoparticles, the black smaller circles indicate the AB conductive additive, and the gray surfaces signify ALD coatings. For simplicity, the schematic follows the evolution of a
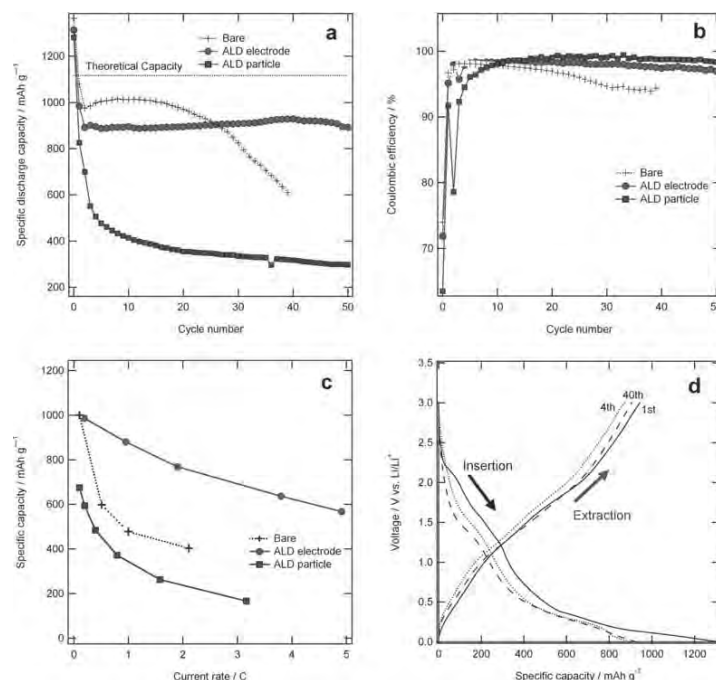

Figure 2. Comparison between bare, 4-cycle ALD coated MoO_3 nanoparticles and 4-cycle ALD coated electrodes in a composition of 70:10:20 (MoO_3:AB:PVDF) for a) cycling stability at C/2 (following two cycles at C/10), b) Coulombic efficiency, c) rate capability and d) voltage profile for ALD coated electrode of nMoO_3.

Table 1. Strain on the ALD alumina surface coating and corresponding deformation for different active materials.

Material	Volume expansion	Experimental capacity [mAhg⁻¹]	Calculated strain	Deformation region
Graphite flakes	10%[32]	372	3.19%	Elastic/Plastic
LiCoO₂	1.5%[33]	170	0.45%	Elastic
Silicon	400%[10]	~3200	70.9%	Fracture
Metal oxides	**100–250%**	**800–1300**	**26–52%**	**Fracture**
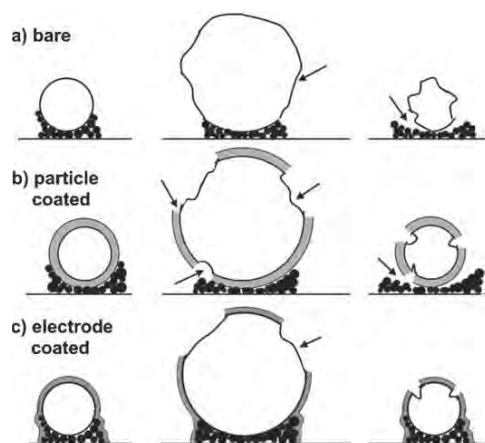
Figure 3. Schematic representation of the effects of volume expansion upon a) bare particles, b) an ALD coated nano-MoO₃ particle and c) a particle from an ALD coated porous electrode.

single nanoparticle, partially surrounded by conductive additive.

Although cracking must occur, the alumina is still able to "knit" the electrode together and retain electric conductivity/ mechanical integrity that is otherwise lost upon the extreme volume expansion/contraction. Unlike the active material, the conductive additive undergoes no change in volume during

cycling. Since MoO₃ is an electrical insulator ($\sim 10^{-11}$– 10^{-8} S cm⁻¹), the AB:MoO₃ interface is extremely important to the overall conductivity and electrical resistance of the electrode facilitating electron transport along the active material surfaces.[23] By growing an ALD surface coating on the pre-fabricated electrodes, the carbon additive may be effectively attached to the active material in spite of ALD cracking as depicted in Figure 3c. This maintains electrical contact with the MoO₃ surface and also delays mechanical degradation. Using similar logic, failure of pristine and CP cells can be attributed to the disintegration of electron and ion transport pathways due to volume expansion.[24] The enhanced CE stability may also be partially attributed to the physical insulation of the MoO₃ from direct contact with the liquid electrolyte due to the partial surface coating even after cracking.

The electronic conductivity of each electrode was studied with electrochemical impedance spectroscopy (EIS). Figures 4a–c depict Bode plots for bare, CE, and CP at different voltages during the first complete discharge/charge cycle. The voltage of each electrode was held constant for one hour prior to EIS tests in order to allow for complete lithium diffusion and volume change. Both the bare and CE displayed similar resistances during initial lithiation to 1.5 V and 0.001 V (volume expansion). However, after subsequent lithium removal to 1.5 V (volume contraction), the bare electrode resistance measured twice that of the ALD coated electrode. This further confirms that the ALD coating helps to maintain an electrical path and good physical contact between the AB and the MoO₃ surface after volume expansion and contraction. Bode plots of the CP show similar resistances in the mid-frequency region at 1.5 V during lithiation, though also includes an additional low-frequency resistive interface. The low-frequency feature, unique
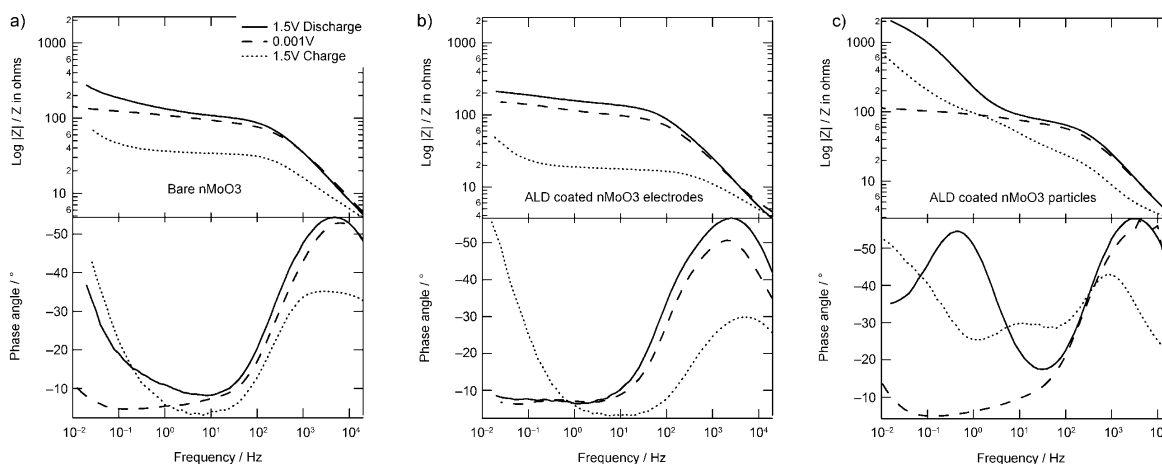
Figure 4. First cycle discharge/charge Bode plots for a) bare b) ALD coated electrode, and c) ALD coated particles.

to the CP, is indicative of the physical interface caused by the Al_2O_3 insulation of the individually coated nanoparticles. The extra resistive layer indicated in Figure 4b decreases ion mobility and limits conductive electron pathways.

Physical contact between MoO_3 nanoparticles and the conductive additive/binder ensures proper electron conduction and is necessary to achieve good cycling stability. If carbothermal reduction to MoO_{3-y} during the electrode pre-heat treatment is observed, it suggests that good conductivity is maintained. This is consistent with previous studies indicating that slightly reduced MoO_{3-y}, that occurs upon ball milling, exhibits enhanced cycling stability.[25] Here the carbothermal reduction occurs upon heat treatment at 250°C in Ar prior to coin cell assembly.[18] When heated, the surface oxygen of MoO_3 reacts with both the melted polymer binder chains ($T_{melt} \sim 170\,°C$), as well as the carbon additive to form CO and CO_2, transforming the active material to a partially oxygen deficient state. The desorbing species that indicate this reaction were previously observed using temperature programmed desorption (TPD).[18]

Differential capacity plots may be employed to determine lithium insertion potentials, and in general, negative peak shifts can be attributed to two factors: kinetics or change in oxidation state. Figure 5 compares the differential capacity
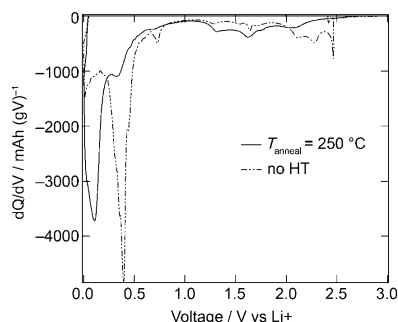

Figure 5. First cycle differential discharge capacity MoO_3 electrodes undergoing no heat treatment and overnight heat treatment (HT) at 250°C.

plots of heat-treated and non-heat treated electrodes. (For this comparison, identical particle sizes and testing conditions were used in order to eliminate kinetics as a possible cause for the voltage shifts.) The initial insertion of lithium into pure MoO_3, represented by the non-heat treated electrode, exists in two distinct phases. The first phase is the intercalation of lithium into Mo–O interplanar octahedral sites that can accommodate approximately $1.5\,Li^+$.[26–28] The second phase, common to transition metal oxides, is the conversion stage described in Equation (1), where MoO_3 undergoes a displacement reaction to form Mo metal and Li_2O creating a highly disordered and amorphous structure at low voltages ($< 1.0\,V$).[25,29] Peaks at potentials greater than 2.0 V are associated with the first phase, lithium intercalation, while the large features below 0.5 V represent the second phase, the conversion reaction. The dashed line in Figure 5, observed for the non-heat treated electrode, is typical of pure MoO_3. The peak attributed to the con-

version reaction is found at 0.4 V. For the heat-treated electrode, the low voltage peak is significantly shifted towards a negative potential indicating MoO_3 reduction. This heat treatment that, enables effective interactions with the conductive additive, was previously shown necessary to achieve stable cycling.[18]

Similar analysis was used to examine the CE and CP. The first cycle differential discharge capacity plots are shown in Figure 6. Again both the CE and CP were subjected to heat
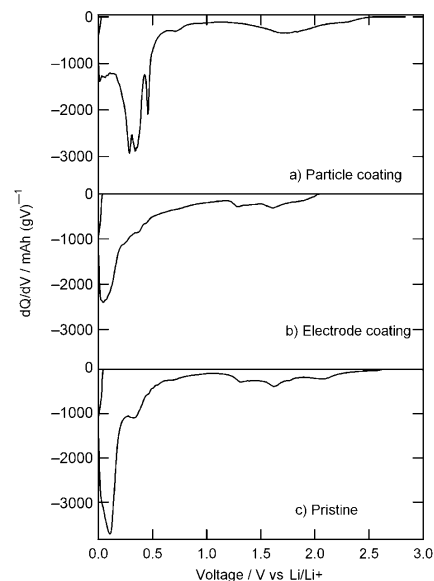

Figure 6. First cycle differential discharge capacity (dQ/dV) at a rate of C/10.

treatment at 250°C prior to coin cell assembly. The CE lithium uptake looks similar to that of the bare sample. Importantly, by coating over the surface of the electrode, the MoO_3 remains capable of undergoing reduction due to the direct contact with AB or binder. The comparable peak positions and heights between bare and CE signify that the active material undergoes no significant chemical change after the coating is applied. The very small difference in peak position of $-0.08\,V$ seen between the pristine and CE is most likely due to slightly slower kinetics through the alumina.[30] Alternately, the CP lithiation potentials show similar characteristics to that of non-reduced, non-heat treated MoO_3 in Figure 5. Unlike the bare heat-treated MoO_3 and CE, the multi-pronged, peak remains close to 0.5 V. This suggests that the ALD coating inhibits the carbothermal reduction by preventing physical contact between the MoO_3 and AB/binder. Thus ALD coatings to the entire electrode are necessary to enable favorable reactions that occur during electrode pre-heat treatment.

ALD coatings were also applied on commercial MoO_3 electrodes. Figure 7 displays results from coating the electrodes of commercially available micron sized MoO_3 with 4 cycles of Al_2O_3 using ALD. Despite the tremendous improvements reported above for coating high surface area nanoparticle electrodes, a similar benefit is not observed for micron-sized parti-
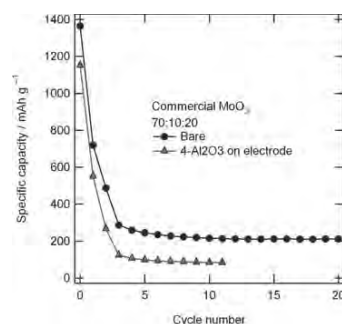
Figure 7. ALD coating effect on cycling performance of commercially available µm-sized MoO₃ particles.

cles. Again the rapid failure of micron-sized particles is due to the extreme fracturing upon volume expansion during cycling.[19] For the micron-sized particles the thin ALD coating is not prolific enough to provide any significant adhesion to the conductive additive. Additionally, the dQ/dV remains unchanged after an overnight 250 °C heat treatment of the micron-sized MoO_3 electrodes. This suggests that high surface areas and extensive contact with the conductive additive are required to most importantly maintain electrical conductivity and achieve reduction to an MoO_{3-y} state.

Finally, it is important to note that all specific capacities are calculated using both the weight of the active material and the weight of the alumina coatings. The viability of passive surface coatings in commercial applications greatly depends upon the total volumetric and gravimetric capacities of the system (active material, conductive additive, binder, coating, etc). The surface coating mass was included in the calculations in order to present an accurate change in total gravimetric capacities. From Figure 2a, 4-layers of alumina on electrodes show that the stable capacity is reduced by ~10% compared to the bare. This is consistent with the fact that the calculated weight of an Al_2O_3 coating that is 4–8 Å thick on an MoO_3 nanoparticle with a diameter of ~40 nm is 7–14 wt%. Thus, at the nanoscale a thin coating is necessary both to achieve high gravimetric capacities and fast ionic conduction.

3. Conclusions

Molybdenum trioxide nanoparticles and electrodes have been coated with Al_2O_3 by ALD and electrochemically tested versus lithium metal from 0.001–3 V. Unlike sol-gel, ALD allows for a uniform coating on both particles and electrodes as well as tailored uniformity for monolayer deposition. Electrodes coated with only 4-monolayers of Al_2O_3 outperform electrodes fabricated from bare nanoparticles as well as particles coated with ALD prior to electrode fabrication. For the coated electrodes a stable capacity of 900 mAh g⁻¹ for 50 cycles at a rate of C/2 is observed and ~600 mAh g⁻¹ is observed at a rate of 5C. The bare sample showed early cycling degradation beginning after only 20 cycles and the particles coated with ALD prior to electrode fabrication deteriorated even more rapidly. When the ALD coating is applied to the entire electrode it creates some

adhesion to the conductive additive allowing for less mechanical degradation from the extreme volume expansion/contraction that occurs upon cycling. Some surface protection against electrolyte reaction may also be achieved even though cracking in the ALD layer must occur. Importantly the ALD coating on the entire electrode allows for carbothermal reduction of the MoO_3 to occur indicating intimate contact between the active material and conductive additive. In addition, the thin ALD coatings do not represent a significant volume or weight fraction of the nanoscale materials. Thus even a brittle Al_2O_3 coating directly on the surface of MoO_3 has been demonstrated to stabilize high volume expansion nanoparticles. Future investigations will be on ALD coatings of more elastic materials.

Experimental Section

Electrode Fabrication: Active material, nano-MoO_3, was obtained using a hot-wire chemical vapor deposition method as described by Riley et al.[18] The deposition chamber was held at 300 °C in a 75 Torr argon atmosphere with a partial pressure of ~7% oxygen. The collected powder was then annealed in air at 300 °C for 2.5 h to obtain a fully oxidized α-MoO_3 sample. Electrodes were made using a 70:10:20 composition of AM:AB:PVDF dissolved in *N*-methyl-2-pyrrolidone. Upon spreading on 20 nm thick Cu foil, the NMP was evaporated at 120 °C for 1 hour in air and then again for 8 h under vacuum. All electrodes were then heat treated at 250 °C on a hot plate in an Ar glove box overnight.

ALD Growth: Al_2O_3 ALD was grown on MoO_3 nanoparticles and on composite electrodes containing MoO_3 nanoparticles, AB and PVDF. ALD on MoO_3 nanoparticles prior to electrode fabrication was performed using a rotary ALD reactor.[31] To perform ALD on powders, the powders were placed in a porous stainless steel cylinder in the reaction chamber. The cylinder was positioned on a magnetically coupled shaft via a load lock door. A rotor turns the cylinder to agitate the powder. A capacitance manometer was used to measure the pressure in the reaction chamber. The introduction of precursor and purge gases was controlled via a series of pneumatic and needle valves. To evacuate the chamber, a gate valve was opened to connect the chamber to a vacuum pump. Once coated, electrodes were constructed using the method described above with the ALD-nano-MoO_3 particles. For electrode coatings, first the electrode was made as described above and subsequently ALD films were deposited. Although the composite electrodes are porous, the internal surfaces are accessible to the ALD precursors.

The Al_2O_3 ALD reaction sequence was: 1) Trimethylaluminum dose to 1.0 Torr; 2) TMA reaction time; 3) evacuation of reaction products and excess TMA; 4) N_2 dose to 20.0 Torr; 5) N_2 static time; 6) evacuation of N_2 and any entrained gases; 7) H_2O dose to 1.0 Torr, 8) H_2O reaction time; 9) evacuation of reaction products and excess H_2O; 10) dose N_2; 11) N_2 static time; and 12) evacuation of N_2 and any entrained gases. This sequence constitutes one cycle of Al_2O_3 ALD. The reactor temperature was 180 °C.

Material Characterization: The Al_2O_3 ALD coated and bare MoO_3 nanoparticles were examined by transmission electron microscopy using a FEI Tecnai F20 UT microscope operated at 200 kV. The presence of Al_2O_3 layer on the surface of MoO_3 nanoparticles was confirmed by nano-probe energy dispersive X-ray spectroscopy.

Electrochemical Testing: All electrodes were electrochemically tested in coin cells (CR2023) using LiPF$_6$ in 1:1 ethylene carbonate: dimethyl carbonate liquid electrolyte and lithium foil as a counter electrode. Coin cells were symmetrically charged and discharged from 0.001 V to 3.0 V with constant current first at a charge/discharge rate of C/10 for 2 cycles, followed by a rate of C/2. For rate study tests, the current was increased after 3 cycles at each pre-designated C-rate. AC impedance was taken for the first cycle when the current, during a voltage hold, dropped below 15 µA, indicating near-charge equilibrium and limited lithium movement across electrodes.

[1] *INEEL FreedomCAR Battery Test Manual For Power-Assist Hybrid Electric Vehicles*, Prepared for the U. S. Department of Energy, **2003**.

[2] H. Li, X. J. Huang, L. Q. Chen, G. W. Zhou, Z. Zhang, D. P. Yu, Y. J. Mo, N. Pei, *Solid State Ionics* **2000**, *135*, 181.

[3] J. M. Tarascon, P. Poizot, S. Laruelle, S. Grugeon, L. Dupont, *Nature* **2000**, *407*, 496.

[4] Y. S. Kim, H. J. Ahn, H. S. Shim, T. Y. Seong, *Solid State Ionics* **2006**, *177*, 1323–1326.

[5] J. Graetz, C. C. Ahn, R. Yazami, B. Fultz, *Electrochem. Solid-State Lett.* **2003**, *6*, A194.

[6] C. Ban, Z. Wu, D. T. Gillaspie, J. L. Blackburn, L. Chen, Y. Yan, A. C. Dillon, *Adv. Mater.* DOI: 10.1002/adma.200904285.

[7] A. L. M. Reddy, M. M. Shaijumon, S. R. Gowda, P. M. Ajayan, *Nano Lett.* **2009**, *9*, 1002.

[8] C. K. Chan, H. L. Peng, G. Liu, K. McIlwrath, X. F. Zhang, R. A. Huggins, Y. Cui, *Nat. Nanotechnol.* **2008**, *3*, 31.

[9] L. Taberna, S. Mitra, P. Poizot, P. Simon, J. M. Tarascon, *Nat. Mater.* **2006**, *5*, 567.

[10] R. Z. Yang, Z. X. Wang, J. Y. Liu, L. Q. Chen, *Electrochem. Solid-State Lett.* **2004**, *7*, A496.

[11] X. Fan, L. Zou, Y. P. Zheng, F. Y. Kang, W. C. Shen, *Electrochem. Solid-State Lett.* **2009**, *12*, A199.

[12] H. Liu, G. X. Wang, J. Park, J. Wang, C. Zhang, *Electrochim. Acta* **2009**, *54*, 1733.

[13] J. Li, H. M. Dahn, L. J. Krause, D. B. Le, J. R. Dahn, *J. Electrochem. Soc.* **2008**, *155*, A812.

[14] Y. M. Kang, S. M. Lee, M. S. Sung, G. J. Jeong, J. S. Kim, S. S. Kim, *Electrochim. Acta* **2006**, *52*, 450.

[15] Y. S. Jung, A. S. Cavanagh, A. C. Dillon, M. D. Groner, S. M. George, S. H. Lee, *J. Electrochem. Soc.* **2010**, *157*, A75–A81.

[16] Y. S. Jung, A. Cavanagh, L. Riley, A. Dillon, M. Groner, S. George, S.-H. Lee, *Adv. Mater.* DOI: 10.1002/adma.200903951.

[17] M. S. Whittingham, *Prog. Solid State Chem.* **1978**, *12*, 41–99.

[18] L. Riley, S.-H. Lee, L. Gedvilias, A. Dillon, *J. Power Sources* **2010**, *195*, 588.

[19] S. H. Lee, Y. H. Kim, R. Deshpande, P. A. Parilla, E. Whitney, D. T. Gillaspie, K. M. Jones, A. H. Mahan, S. B. Zhang, A. C. Dillon, *Adv. Mater.* **2008**, *20*, 3627.

[20] A. C. Dillon, A. H. Mahan, R. Deshpande, R. Parilla, K. M. Jones, S. H. Lee, *Thin Solid Films* **2008**, *516*, 794.

[21] M. D. Groner, F. H. Fabreguette, J. W. Elam, S. M. George, *Chem. Mater.* **2004**, *16*, 639.

[22] D. C. Miller, R. R. Foster, Y. D. Zhang, S. H. Jen, J. A. Bertrand, Z. X. Lu, D. Seghete, J. L. O'Patchen, R. G. Yang, Y. C. Lee, S. M. George, M. L. Dunn, *J. Appl. Phys.* **2009**, *105*, 093527.

[23] N. Kumagai, K. Tanno, *J. Appl. Electrochem.* **1988**, *18*, 857.

[24] S. D. Beattie, D. Larcher, M. Morcrette, B. Simon, J. M. Tarascon, *J. Electrochem. Soc.* **2008**, *155*, A158.

[25] Y. S. Jung, S. Lee, D. Ahn, A. C. Dillon, S. H. Lee, *J. Power Sources* **2009**, *188*, 286.

[26] N. A. Chernova, M. Roppolo, A. C. Dillon, M. S. Whittingham, *J. Mater. Chem.* **2009**, *19*, 2526.

[27] P. G. Dickens, G. J. Reynolds, *Solid State Ionics* **1981**, *5*, 331.

[28] J. Swiatowska-Mrowiecka, S. de Diesbach, V. Maurice, S. Zanna, L. Klein, E. Briand, I. Vickridge, P. Marcus, *J. Phys. Chem. C* **2008**, *112*, 11050.

[29] J. O. Besenhard, J. Heydecke, H. P. Fritz, *Solid State Ionics* **1982**, *6*, 215–224.

[30] Y. S. Jung, K. T. Lee, S. M. Oh, *Electrochim. Acta* **2007**, *52*, 7061.

[31] J. A. McCormick, B. L. Cloutier, A. W. Weimer, S. M. George, *J. Vac. Sci. Technol. A* **2007**, *25*, 67.

[32] T. Ohzuku, Y. Iwakoshi, K. Sawai, *J Electrochem. Soc.* **1993**, *140*, 2490.

[33] J. N. Reimers, J. R. Dahn, *J. Electrochem. Soc.* **1992**, *139*, 2091–2097.